# SMALL SPECIMEN TEST TECHNIQUES FOR EVALUATING RADIATION-INDUCED CHANGES IN MECHANICAL PROPERTIES

By

Ellen M. Rabenberg

A thesis

submitted in partial fulfillment

of the requirements for the degree of

Master of Science in Materials Science & Engineering

Boise State University

December 2012

© 2012

Ellen M. Rabenberg

ALL RIGHTS RESERVED

BOISE STATE UNIVERSITY GRADUATE COLLEGE

# DEFENSE COMMITTEE AND FINAL READING APPROVALS

of the thesis submitted by

Ellen M. Rabenberg

Thesis Title: Small Specimen Test Techniques for Evaluating Radiation-Induced Changes in Mechanical Properties

Date of Final Oral Examination: 5 October 2012

The following individuals read and discussed the thesis submitted by student Ellen M. Rabenberg, and they evaluated her presentation and response to questions during the final oral examination. They found that the student passed the final oral examination.

| | |
|---|---|
| Darryl P. Butt, Ph.D. | Chair, Supervisory Committee |
| Rick Ubic, Ph.D. | Member, Supervisory Committee |
| Frank A. Garner, Ph.D. | Member, Supervisory Committee |

The final reading approval of the thesis was granted by Darryl P. Butt, Ph.D., Chair of the Supervisory Committee. The thesis was approved for the Graduate College by John R. Pelton, Ph.D., Dean of the Graduate College.

## ACKNOWLEDGMENTS

This research conducted was funded by a Laboratory Directed Research and Development (LDRD) grant through Battelle Energy Alliance. The setup and analysis of the mechanical testing presented could not have been accomplished without the help of many people. First, I would like to thank my committee members; Dr. Darryl Butt, Dr. Frank Garner, and Dr. Rick Ubic; for their support and guidance through this thesis. I thank Dr. Bulent Sencer of Idaho National Laboratories for his help acquiring equipment and expertise with the materials tested and the miniaturized test techniques. This research could not have been accomplished without the support of the Advanced Materials Laboratory at Boise State University, particularly Brian Jaques, Kyle Knori, Kyle Witherspoon, and Allyssa Bateman.

Paula Freyer from Westinghouse Electric Company LLC was instrumental in obtaining material for the irradiated work. The infrastructure for conducting shear punch tests of the irradiated material could not have been done without the help and expertise of the team at the Center for Advanced Energy Studies, including Bryan Forsmann, Dr. Kerry Allahar, Joanna Taylor, and Kristi Moser-Mcintire.

Finally, I would like to thank my parents and sister for their love and support of my education.

ABSTRACT

Small Specimen Test Techniques for Evaluating Radiation-Induced Changes in Mechanical Properties

Ellen M. Rabenberg

The mechanical properties of as-received and irradiated 304 stainless steel (304SS) were evaluated by the shear punch and miniature tensile techniques. A purpose of this study was to evaluate the shear punch technique itself, which is a less developed technique versus miniature tensile testing. This was accomplished in part by comparing yield and ultimate strengths obtained from shear punch and miniature tensile data. The tests were further correlated by evaluating the mechanical properties of aluminum 6061 and Inconels 600 and 718. A linear relationship was observed between the shear strength and tensile strength data, providing a correlation between the two test methods.

The influences, if any, of specimen surface roughness, thickness, and material irradiation history on mechanical properties were evaluated. Through shear punch and miniature tensile testing techniques involving annealed 304 stainless steel, it was demonstrated that surface roughness had no influence on the observed mechanical properties. For T6 aluminum 6061, increased sample thickness lead to decreased ductility while yield and ultimate strengths were similar across the thickness range chosen. The results of specimen surface roughness and

thickness experiments show minimal surface preparation is required for accurate strength measurements. The minimum thickness required for shear punch testing is 200 $\mu m$.

It is demonstrated that with increased irradiation damage, the strength determined through shear punch testing of 304SS increases. Increased temperature from gamma heating was shown to decrease strength, likely due to annealing at the higher temperatures. A ferroprobe technique was developed to assess whether the changes in strength were due to irradiation damage or thermal gradients or from a martensitic transformation induced during shear punch testing. Similar ferromagnetic measurements at each irradiation and temperature condition suggest a low saturation in the formation of martensite during shear punch testing with increasing irradiation damage.

TABLE OF CONTENTS

LIST OF TABLES

LIST OF FIGURES

# 1 INTRODUCTION

## 1.1 Motivation for Research

Techniques for determining mechanical properties of materials have been miniaturized for many reasons. Two such reasons are to accommodate materials where availability is limited or those that are dangerous to handle in large quantities, such as material that is radioactive. The latter was the primary motivation for this research. In order to explore the effect of irradiation damage and temperature on strength properties, a miniaturized technique called the shear punch test was used in this research.

The shear punch test is similar to a blanking process where a flat-tipped cylindrical pin shears through the center of a disk-type specimen [2–15]. Experimental results are comparable to standard tensile tests such that the stress-strain curves have similar characteristics. Both include an initial linear elastic region, a non-linear plastic region, maximum strength, and decrease in load until failure. By analyzing these regions in a shear punch curve, certain material properties can be determined, such as shear yield strength, shear ultimate strength, and work hardening exponent [2, 5–10, 12, 15, 16]. Shear strengths can linearly translate into tensile strengths [2–11], allowing comparisons in properties from the shear punch test to properties obtained from larger, standard techniques (such as tensile experiments).

## 1.2 Objectives

This research had three primary objectives. The first was to further develop and standardize the shear punch technique. This was necessary as various shear punch test

geometries and evaluation techniques have been employed to determine a material's strength [2–9, 11, 12, 14, 15], including different punch diameters, punch-die clearances, strain calculations, and shear yield strength determinations. Since the fixturing was predetermined in this study (eliminating the need to standardize test geometry), the focus was on standardizing strain and yield strength calculations for the shear punch test. Additionally, a correlation for yield and ultimate strengths was determined for the shear punch and miniature tensile techniques. The correlation was drawn by comparing strengths obtained through the shear punch and miniature tensile techniques with 304SS, aluminum 6061, and Inconels 600 and 718.

The second objective of the research presented here was to further correlate the shear punch and miniature tensile tests by determining the effect of specimen surface roughness and thickness on the stress-strain curve behavior for both test techniques. The effect of surface roughness was done to see whether grinding and polishing steps were required to obtain reliable and repeatable results. The effect of specimen thickness was tested to determine the minimum thickness required for the shear punch and miniature tensile tests.

The third objective of this research was to determine how irradiation damage and temperature affect the strength of 304SS through shear punch testing. As the material used for testing irradiation effects is susceptible to strain-induced martensitic transformations, a non-destructive technique was developed to detect martensite during shear punch testing. Martensitic transformations may be important in nuclear reactor steels as the transformation may allow increased ductility when the metal is exposed to high levels of radiation [17]. Increased ductility may allow reactors to run safely at higher temperatures for longer periods

of time, extending the reactor's working lifetime, as the probability of the structure failing through brittle failure is reduced.

# 2 BACKGROUND INFORMATION

The uniaxial tensile test is a common technique for determining the strength of materials [18–20]. The tensile test consists of the lengthening of a material of a specified geometry [18]. The geometries are typically either rectangular or cylindrical and are defined in the ASTM standard E 8M-04 [1].

During a tensile test, changes in applied load $P$ and specimen length $\Delta l$ are measured [18–20]. From these values, a stress-strain curve can be generated using the equations:

$$\sigma = engineering\ stress = \frac{P}{A_0} \tag{2.1}$$

$$\epsilon = engineering\ strain = \frac{\Delta l}{l_0} = \frac{l_f - l_0}{l_0} \tag{2.2}$$

where $P$ is applied load, $A_0$ is initial specimen cross-sectional area, $l_f$ is the final gage length, and $l_0$ is the initial gage length.

Figure 2.1 shows a typical engineering stress-strain curve obtained for metals. The curve has an initial linear elastic region, where the slope is defined as the Young's modulus of elasticity $E$. As dislocations within the material begin to move, the curve deviates from linearity into a non-linear plastic region. The point at which the deviation occurs is known as the yield stress. The yield stress is calculated using a $0.2\%$ strain offset from linearity. Once the curve flattens to a slope of zero (refered to as the ultimate strength), localized necking occurs as onset to fracture is approached. Some of the materials properties typically reported are yield strength, ultimate strength, Young's modulus, and ductility [1, 18–20].

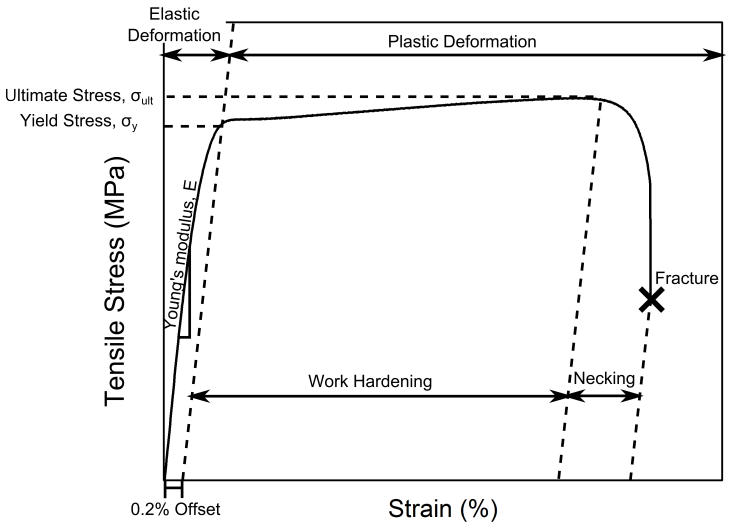


**Figure 2.1:** Typical engineering stress-strain curve for metals noting Young's modulus, offset used for calculating yield stress, yield stress, and ultimate stress.

## 2.1 Shear Punch Test

Another testing technique that gives similar materials information as the tensile test is the shear punch test. The shear punch test is a non-standard technique that is similar to a blanking operation [2–15]. The test consists of a cylindrical punch shearing a fraction of a round specimen into a receiving die, as shown in Figure 2.2. During the test, applied load $P$ and punch displacement $\Delta d$ are measured. These two measured values can be used to calculate stress and strain.

The applied load and punch displacement measurements are used to calculate shear stress as

$$\tau = engineering\ shear\ stress = \frac{P}{2\pi r_{ave} t} \tag{2.3}$$

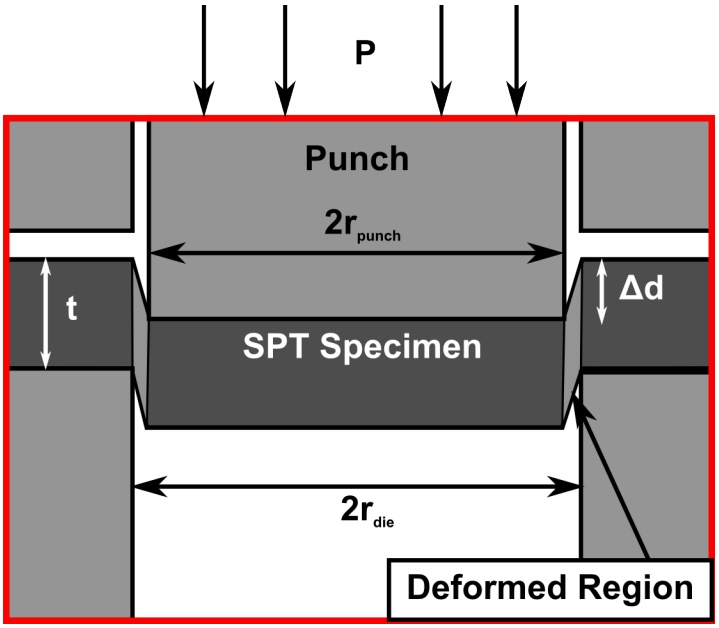


**Figure 2.2:** Description of shear punch test.

where $P$ is the applied load, $r_{ave}$ is the average radius of the punch ($r_{punch}$) and receiving die ($r_{die}$), and $t$ is the specimen thickness [2–7, 10–15]. The $2\pi r_{ave}t$ value is the cross-sectional area corresponding to the deformed region of the shear punch sample, similar to the $A_0$ value of Equation 2.1.

Strain is defined as the change in length divided by the initial length, defined in Equation 2.2. For the shear punch test, shear strain has been defined in a few ways. In one method, the initial length $l_0$ was taken as the difference in the radii of the punch and receiving die, making shear strain equal to $\epsilon = \Delta d/(r_{die} - r_{punch})$ [8, 14, 15]. The resulting stress-strain curves using this definition of shear strain were dependent on specimen thickness. The curves obtained using thick specimens have different elastic slopes than those obtained using thinner specimens. This difference in elastic slopes also affected the yield strength calculations as yielding was perceived to occur at different strains.

To compensate for differences in curve behavior with differing specimen thicknesses, some authors defined shear strain as

$$\epsilon = normalized\ displacement = \Delta d/t \tag{2.4}$$

where $\Delta d$ is the punch displacement and $t$ is specimen thickness [2, 3, 6, 12, 16]. By using the normalized displacement definition for strain, the linear region of the stress-strain curve obtained using specimens with different thicknesses were similar. Additionally, yield strength calculations were similar with varying specimen thickness as yielding was perceived to occur at similar strains.

### 2.2 Comparisons Between Uniaxial Tensile and Shear Punch Experiments

While similarities exist between the materials properties obtained through the tensile and shear punch techniques, the two cannot be directly correlated. As observed in literature, a lower stress is required to fracture a shear punch specimen as compared to tensile experiments. The reason for this lies in differences in the stress state of the material for each test. For the uniaxial tensile test, the stress tensor is

$$\begin{pmatrix} \sigma_1 & 0 & 0 \\ 0 & 0 & 0 \\ 0 & 0 & 0 \end{pmatrix} \tag{2.5}$$

Assuming deformation is not impeded by outside forces in the shear punch test, the material is theoretically placed in a pure shear stress state, described by

$$\begin{pmatrix} 0 & \tau_{12} & 0 \\ \tau_{21} & 0 & 0 \\ 0 & 0 & 0 \end{pmatrix} \tag{2.6}$$

where $\sigma_{12}$ equals $\sigma_{21}$.

The equivalent stress for each defined stress state can be calculated using the Von Mises yield criterion, which states [18]:

$$\sigma_{eq,M} = \sqrt{\frac{1}{2}\left[(\sigma_1 - \sigma_2)^2 + (\sigma_1 - \sigma_3)^2 + (\sigma_2 - \sigma_3)^2\right] + 3(\tau_{23}^2 + \tau_{13}^2 + \tau_{12}^2)} \tag{2.7}$$

The equivalent stress defined in Equation 2.7 can be solved in general terms for both the tensile and shear punch stress states. Because the equivalent stresses obtained through both test techniques should be equal for a given material, the quantities can be set equal to one another and solved in terms of tensile stress, $\sigma$, and shear stress, $\tau$.

$$\begin{aligned} \sigma_{eq,M,tensile} &= \sigma_{eq,M,shear} \\ \sigma_1 &= \sqrt{3}\tau_{12} \\ \sigma_1 &= 1.73\tau_{12} \end{aligned} \tag{2.8}$$

Various authors have compared this derived tensile-to-shear stress ratio to experimental results [2–10]. This was accomplished by comparing the tensile and shear punch strengths tested using a variety of low, medium, and high strength materials. Regardless of the materials compared, a linear trend was observed. Yield strength ratios varied between 1.67 - 2.3 [2–10] and ultimate strength ratios varied between 1.29 - 2.042 [2, 5–7, 9].

The empirical correlation between tensile and shear strengths is also used to determine the optimum offset for determining shear yield stress as there is not a standard strain offset used between authors. Authors have varied the offset from approximately 0.2% [6, 16] and 1% [2, 3, 5, 8, 10]. These experimentally determined offsets were established by plotting tensile yield stress (calculated using a 0.2% strain offset) verses shear yield stress calculated with various shear strain offsets. The offset that allowed the least deviation from linearity was used to calculate shear yield stress [2, 3, 5, 6, 8, 10, 16]. Finite element analysis studies suggest die compliances affect measurements [3]. However, little has been reported on other factors that might influence shear punch results.

## 2.3 Factors Influencing Miniature Tensile and Shear Punch Stress-Strain Curve Behavior

When transitioning from bulk material properties obtained through tensile experiments to the small scale of the shear punch test, surface characteristics may have a greater impact on the measured properties. To ensure the accuracy of data when investigating irradiation damage and thermal gradient effects, as reviewed in Sections 2.3.3 and 2.3.4, surface roughness and thickness effects were studied. Once it was known how specimen thickness and surface roughness affected the measured data, the shear punch test was used to correlate the effect of irradiation damage and temperature on austenitic stainless steels. As austenitic steels are susceptible to strain-induced martensitic transformations, a non-destructive ferromagnetic measurement technique was developed to detect transformed martensite.

### 2.3.1 Surface Roughness

In shear punch experiments, surface roughness has been reported to minimally affect strength measurements [2]. Surface roughness effects were studied further, though, to ensure

accurate analysis when determining irradiation effects, discussed in Sections 2.3.3 and 2.3.4. This concern came about when the shear punch specimens obtained for testing the irradiation effects were received in a "rough" surface condition from polishing with 600 grit SiC papers. A study by Guduru *et al.* [2] noted varying surface finish minimally impacted strength measurements although this was not discussed in much detail.

### 2.3.2 Specimen Thickness

The effect of specimen thickness has been explored extensively for the shear punch test and has shown yield and ultimate strengths are not affected by specimen thickness [6, 15, 16]. As different geometries have been used by different authors, this study investigated the thickness effect for a 1 mm diameter punch geometry with the goal of determining the minimum thickness required to obtain repeatable results. Reproducibility was particularly important when transitioning to the limited radioactive material obtained to explore irradiation effects. While material is typically available to repeat tests involving non-irradiated materials, a limited quantity of irradiated specimens were obtained.

Ductility correlations were also investigated to determine the impact of specimen thickness on stress-strain curve behavior. If specimen thickness was not shown to impact ductility, large unexpected variations in curve behavior might indicate further investigations are needed to explain the behavior.

An example of this was the discovery of martensite forming in irradiated austenitic steel exposed to high levels of radiation [17, 21–23] and is discussed more in depth in Section 2.3.4. Abnormally large increases in ductility was observed for exposures of 26 and 55 dpa as compared to material exposed to lower amounts of radiation when the material was expected

to exhibit brittle behavior. Further investigations revealed the large increases in ductility corresponded to the formation of martensite during the tensile experiment.

As the present study involved testing 304SS, a material known to be susceptible to strain-induced martensitic transformations [24, 25], the ability to correlate large variations in ductility to a potential martensitic transformation rather than specimen thickness would be beneficial.

### 2.3.3 Irradiation Damage

Irradiation damage occurs when energy is transfered from highly energized bombarding particles, typically neutrons, to the target material. As energy is transferred, atoms are displaced in the lattice. These displaced atoms, referred to as primary knock-on atoms, in turn displace more atoms. These bombardments cascade through the material until the energy is dissipated. The overall damage from irradiation is typically reported in terms of dose, the average number of displacements each atom has been displaced (i.e., displacements per atom, dpa).

As the damage cascade occurs, various defects are formed including defect clusters, dislocation loops, voids and bubbles, and precipitates [20, 26]. Typical characteristics of metal exposed to increasing levels of radiation are increased strength, decreased ductility, and decreased work hardening. This occurs because dislocation motion is impeded by the defects formed during radiation exposure.

### 2.3.4 Strain-Induced Martensitic Transformations in Metastable Steels

While many defects are formed during the irradiation event, changes in microstructure may also form during mechanical testing, as briefly mentioned in Section 2.3.2. In room-temperature tensile experiments by Gusev *et al.* [17, 21–23], investigation into phase

transformations during testing was sparked when the stress-strain curve showed an irregular extended plateau. This irregularity corresponded to an approximately 20-40% total strain. For the austenitic stainless steel tested, which was irradiated to 26 and 55 dpa, a total strain of ≈6-7% was expected for these irradiation exposures. Through microscopy and ferromagnetic measurements, the irregularity was determined to be from a deformation-induced transformation from $\gamma$ austenite to $\alpha$' martensite [17, 21–23].

The $\gamma$ austenite to $\alpha$' martensite phase transformation occurs through a rearrangement in atomic structure from an FCC to BCC stacking [27, 28]. The rearrangement is a result from the interaction of a traveling dislocation with other dislocations or defects in the atomic structure. If the traveling dislocation becomes pinned, it might dissociate into $a_{fcc}/6\ \langle 112 \rangle$ Shockley partial dislocations.

The transformation from FCC to BCC occurs in two processes, as described by Bogers and Burgers [28]. In the first process, a Shockley partial dislocation is "spread" over three consecutive $(111)_{fcc}$ planes. Figure 2.3 (a) defines three (111) planes in the FCC structure that are affected by the transformation. Figure 2.3 (b) shows the three $(111)_{fcc}$ planes stacked upon one another, as seen looking down the [111]. During the transformation, the three consecutive $(111)_{fcc}$ planes are displaced by $a/18\ \langle 112 \rangle$ (1/3 the magnitude of the $a/6\ \langle 112 \rangle$ Shockley partial dislocation) such that the atoms in each $(111)_{fcc}$ plane are stacked along the row of atoms underneath, as shown in Figure 2.3 (c).

As the first transformation process does not form a truly BCC structure, the second process involves shifting the atoms of the stretched $(111)_{fcc}$ planes, shaded in Figure 2.4 (a). This shaded plane is similar to the $(110)_{bcc}$ plane in the BCC structure, shaded in Figure 2.4 (b), though the atoms along the $[110]_{bcc}$ are shifted slightly, as shown in Figure 2.4 (c). In the

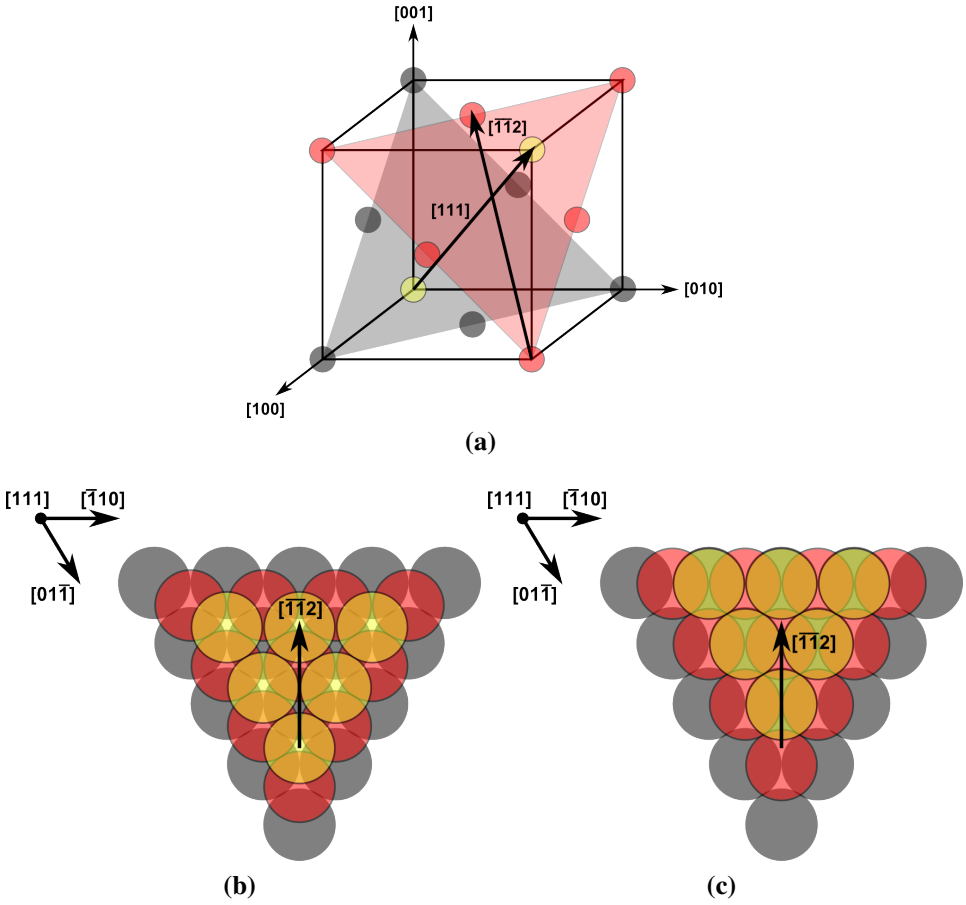


**Figure 2.3:** Schematic of first process in martensitic transformation where individual $(111)_{fcc}$ planes are displaced by $a_{fcc}/18\ \langle 112 \rangle$ where (a) shows the (111) planes in the fcc structure, (b) is a view of the $(111)_{fcc}$ planes along the [111], and (c) is the structure after three planes are displaced by $a_{fcc}/18\ \langle 112 \rangle$.

second shear process, the $(110)_{bcc}$ planes shift by $a_{bcc}/8$ $\langle 110 \rangle$ such that the atoms in each $(110)_{bcc}$ plane are stacked along the row of atoms directly underneath, as shown in Figure 2.4 (d). This slight shift transforms the structure into the BCC structure.

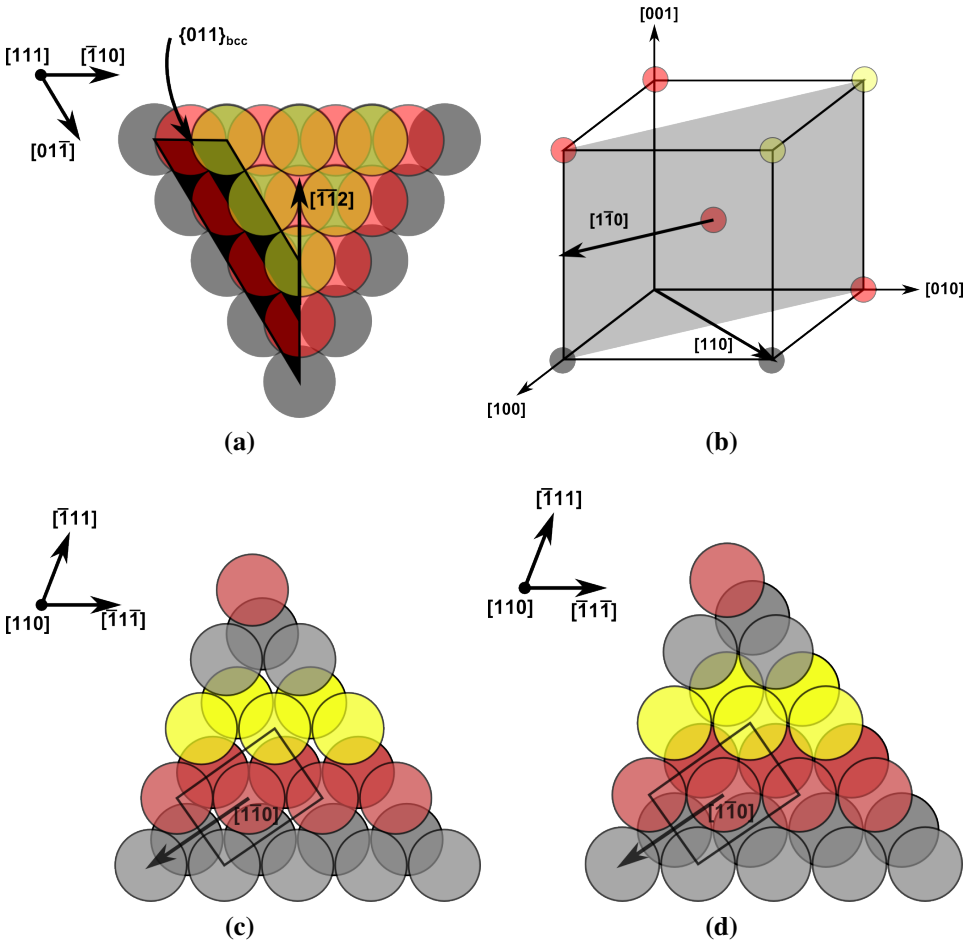


**Figure 2.4:** Schematic of second process in martensitic transformation where individual $(110)_{bcc}$ planes are displaced by $a_{bcc}/8\ \langle 110 \rangle$ where (a) shows which stretched $(111)_{fcc}$ plane (shaded) is equal to $(110)_{bcc}$, (b) shows the $(110)_{bcc}$ planes in the BCC lattice with respect to the BCC lattice, where atoms of similar shading are related to the $(111)_{fcc}$ planes of the first shear process, (c) is a view of the $(110)_{bcc}$ planes along the [110], and (c) is the structure after the planes are displaced by $a_{bcc}/8\ \langle 110 \rangle$.

# 3 EXPERIMENTAL METHODS

## 3.1 Miniature Tensile Testing Setup

A miniaturized version of the sheet-type, dog-bone specimen defined in the ASTM standard E 8M-04 [1] was used for testing, referred to in this thesis as "miniature tensile" specimens. The miniature tensile specimens had a reduced length of 5 mm and a gage width of 1.22 mm. The overall size of the miniature specimens are compared to the full size counterparts in Figure 3.1. An image of the miniaturized specimens used in comparison to a dime is shown in Figure 3.2.

Miniature tensile experiments were carried out on an Instron 5967 electromechanical test frame with a wedge-grip fixture. A tool was developed to ensure proper alignment of the specimens within the grips. Displacement was measured using the frame crosshead measurement. Tests were conducted at room temperature using a $3.3 \times 10^{-3}$ $s^{-1}$ strain rate. Four specimens were tested to failure for each material and processing condition.

## 3.2 Shear Punch Testing Setup

Shear punch experiments were carried out on an Instron 5967 electromechanical test frame, similar to the miniature tensile experiments. An image of the shear punch fixture is shown in Figure 3.3. The shear punch fixturing included a 1 mm diameter flat-end punch, which sheared a portion of a 3 mm diameter specimen into a 1.02 mm hole in the receiving die, as shown in Figure 3.4. Punch tip displacement was measured using a linear variable differential transformer (LVDT) with a $\pm$3.2 mm range attached to the test frame, shown in

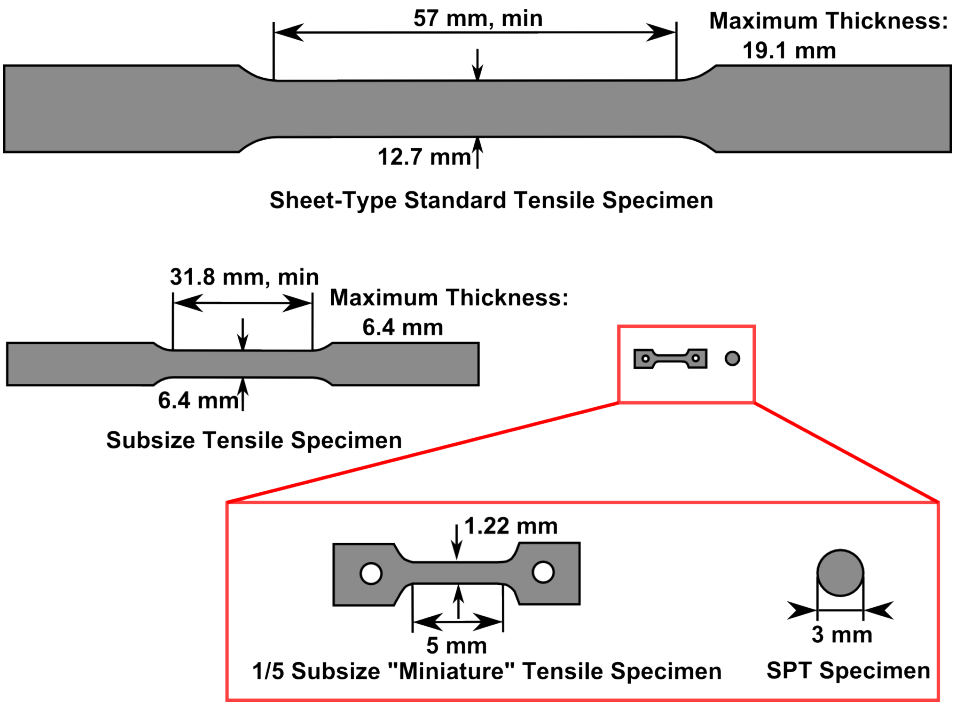


**Figure 3.1:** Schematic of miniature tensile and SPT specimens with gage information as compared to standard tensile specimen sizes defined in the ASTM E8 Standard [1].

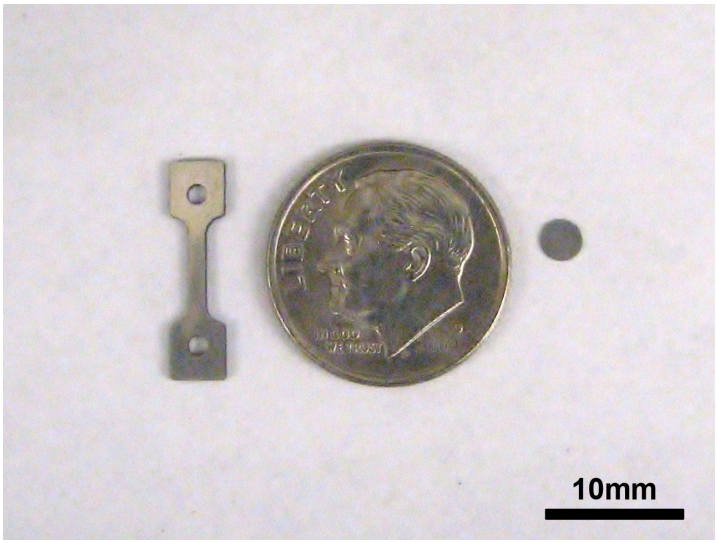


**Figure 3.2:** Comparison of miniature tensile and shear punch specimens with respect to a dime.

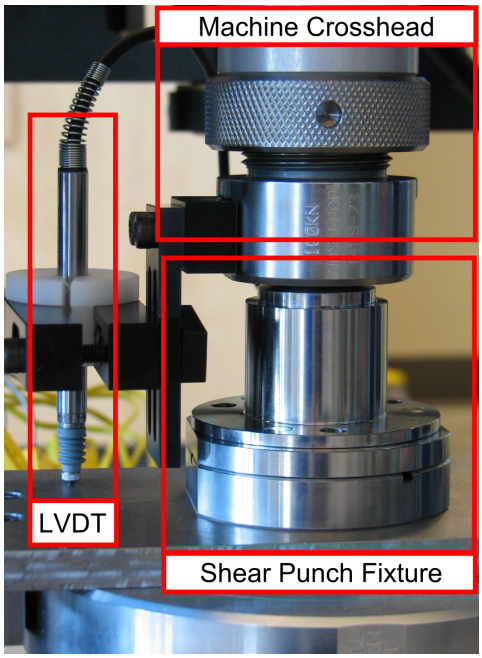


**Figure 3.3:** Image of the shear punch fixture used in this study where the LVDT measures displacement.

Figure 3.3. Tests were conducted at room temperature using a 4 $\mu m/s$ displacement rate. Six specimens were tested to failure for each material and processing condition.

## 3.3 Material and Methods for Determining Correlations Between Miniature Tensile and Shear Punch Experiments

### 3.3.1 Non-Radioactive Materials

Four different non-radioactive materials were tested to correlate properties obtained through the miniature tensile and shear punch techniques. Two different heat treated conditions were tested for each material. The materials and corresponding treatments tested are listed in Table 3.1.

Heat treatments were performed prior to specimen machining according to treating procedures listed in the ASM Metals Reference Book [29]. After treating, individual miniature tensile specimens were electrically discharge machined (EDM) from stock thickness material

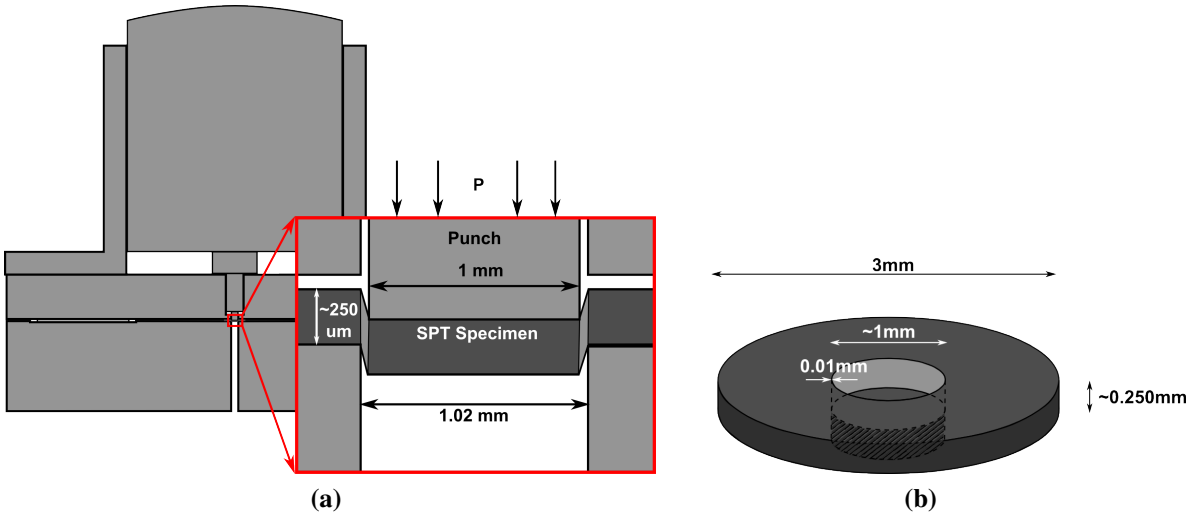


**Figure 3.4:** Schematic of the shear punch fixture where (a) notes the dimensions of the punch and (b) notes the dimensions of a specimen after shear punch testing.

**Table 3.1:** Non-Radioactive Materials and Corresponding Heat Treatments Tested

| Material | Treated Conditions | Treatment Procedure |
|---|---|---|
| 304SS | Annealed | As received from vendor |
| | Treated | As received from vendor |
| Aluminum 6061 | T0 | In accordance with [29] |
| | T6 | As received from vendor |
| Inconel 600 | Annealed | In accordance with [29] |
| | Solution Treated | In accordance with [29] |
| Inconel 718 | Annealed | In accordance with [29] |
| | Aged | In accordance with [29] |

obtained from the vendor. Individual shear punch specimens were fabricated by either EDM or disk-punching 3 mm disks from appropriate stock thicknesses as described in Sections 3.3.2 and 3.3.3.

### 3.3.2 Surface Roughness Effects on Miniature Tensile and Shear Punch Experiments

The effect of surface roughness was studied to ensure accurate analysis when exploring irradiation effects. Testing was accomplished using non-radioactive annealed 304SS that was of similar grade to that of the material tested in the irradiation experiments, as described in Section 3.4.1. Four different surface finishes were tested. Specimens polished with 600 and 800 grit SiC paper and 0.5 $\mu m$ diamond paste were compared to the as-received surface finish from the vendor. These finishes are shown in Figure 3.5. The direction of scratches of the final polishing step were oriented parallel to the specimen gage for the miniature tensile specimens. Since the punch and specimens for the shear punch test are round, scratch orientation was irrelevant.

### 3.3.3 Thickness Effects on Miniature Tensile and Shear Punch Experiments

The effect of specimen thickness was studied to determine the minimum thickness required for accurate property determinations. This was accomplished by testing T6 treated aluminum 6061, one of the lowest strength materials chosen for experimentation. Aluminum 6061 had the highest probably of being affected by specimen thickness as compared to the higher strength 304SS used in the studying surface roughness and irradiation effects. For miniature tensile experiments, specimens were 0.8, 1.0, and 1.2 mm thick. Shear punch specimens were 100, 150, 200, 250, and $300\ \mu m$ thick. The miniature tensile specimens were EDM'd out of stock thickness material obtained from the vendor. Individual shear punch specimens were polished to the appropriate specimen thickness after machining.

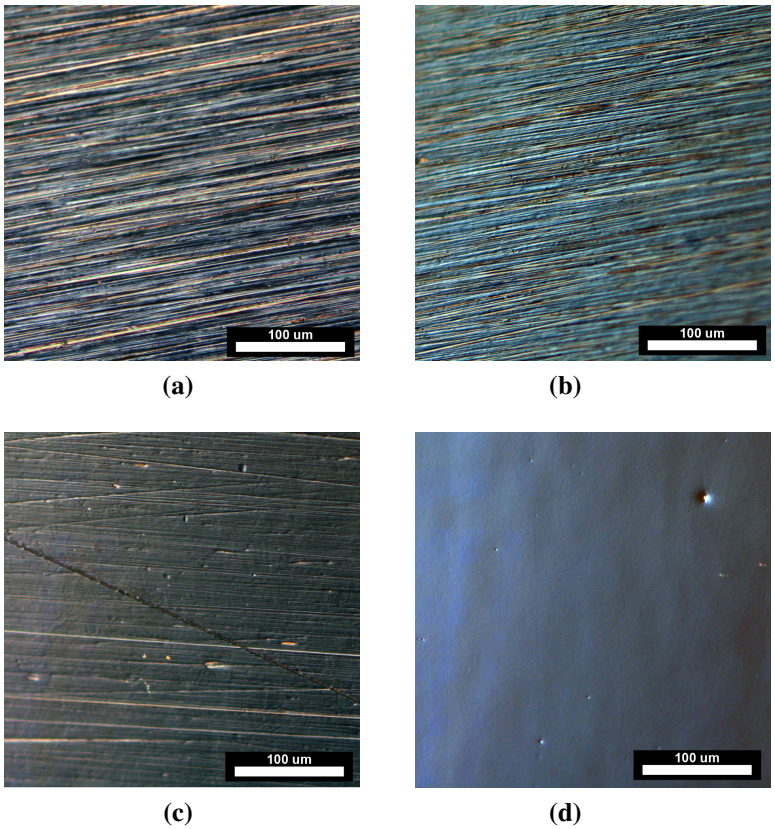


**(a)** **(b)**

**(c)** **(d)**

**Figure 3.5:** Images showing the (a) 600 and (b) 800 SiC grit, (c) as-received from vendor, and (d) $0.5\ \mu m$ diamond surface finishes tested.

## 3.4 Material and Methods for Determining Irradiation Effects

### 3.4.1 Irradiated Stainless Steel

To study the effect of irradiation damage and temperature, shear punch specimens were obtained from two solid 304SS hexagonal (hex) blocks used as neutron reflectors in the now decommissioned Experimental Breeder Reactor II (EBR-II) located at the Idaho National Laboratory (INL) facility located in Idaho Falls, ID. Within the reflector region of the reactor there were many reflector assemblies whose purpose was to reflect escaping neutrons back into the active core. In each reflector assembly there were five 51 mm (2 in) wide hex blocks of various lengths stacked upon one another, shown in Figure 3.6. The assembly used to supply specimens for this study was located just outside the active core in Row 8.

The top (#5) block and center (#3) block were investigated in this study. These two blocks represented a low and high neutron irradiation damage state, respectively. Block 5 was 214 mm long and was located well above the active core, receiving a lower range of neutron dose. Specimens were obtained from both the top and bottom of Block 5, marked in Figure 3.6. Block 3 was 245 mm long and was vertically centered with respect to the core center plane, receiving the largest neutron dose at its center. Specimens were obtained from the center of Block 3, marked in Figure 3.6. The doses were defined in units of dpa (displacements per atom) and values are shown in Table 3.2.

Two "hex coins" were cut from Block 3 and four were from Block 5, marked in Figure 3.6. Strips were then cut from the coins such that all positions along the strip had the same dpa level. Shear punch specimens were machined from three different depths along the strips: 13 mm (0.5 in), 25 mm (1 in), and 38 mm (1.5 in), marked in Figure 3.6. Although the dose did not vary along the strip, the temperature rose along the longer edge of each strip, peaking

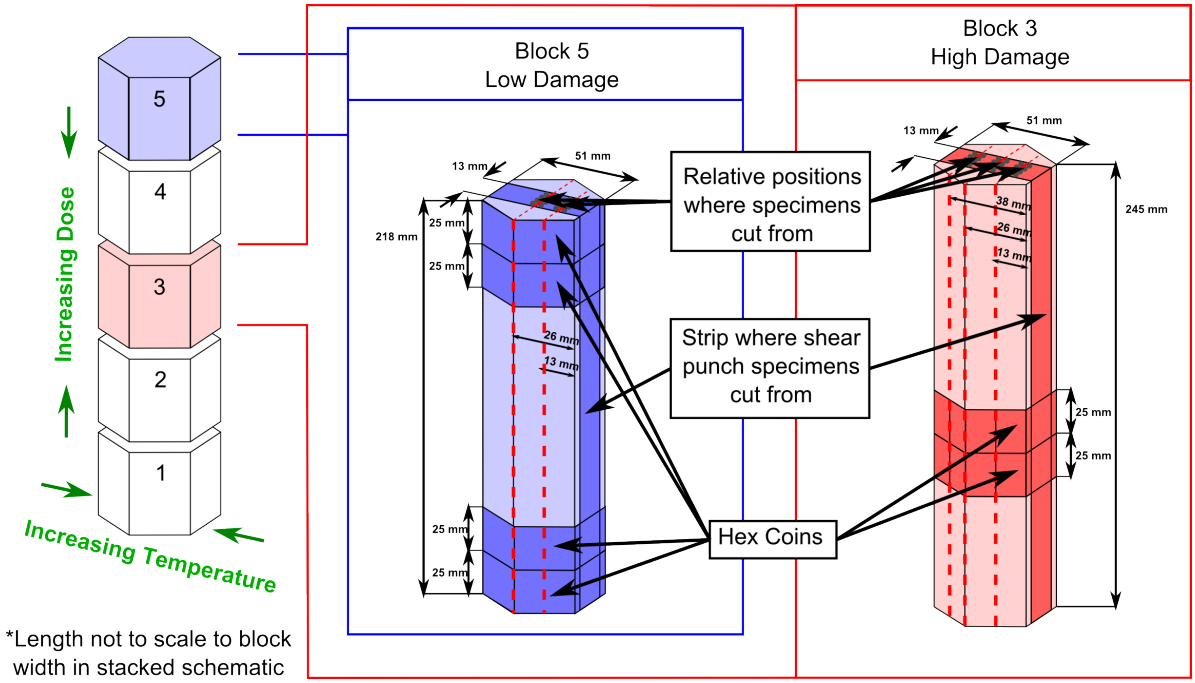


**Figure 3.6:** (Left) Schematic representing the stack of five hexagonal blocks used as neutron reflectors in the EBR-II reactor. The length of the blocks in this stacked schematic is shortened for illustration purposes. Marked is an increasing temperature dependence from the outside face to center of the individual blocks and an increasing dose is observed from the top and bottom of the stack towards the center. Center Detailed description of the hex coins and relative positions (depths) from which specimens came from in low dose Block 5. Right Detailed description of the hex coins and relative positions (depths) from which specimens came from in high dose Block 3.

**Table 3.2:** Description of SPT specimen positions within #3 and #5 hex blocks. Organized in order of increased slice irradiation damage.

| Hex Coin | Irradiation Damage (dpa) | 25 mm Depth Temperature (°C) | 13 mm and 38 mm Depth Temperature (°C) |
|---|---|---|---|
| Unirr | 0 | N/A | N/A |
| 5D | 0.3 | 416 | 415 |
| 5C | 0.5 | 415 | 415 |
| 5B | 3 | 420 | 416 |
| 5A | 4 | 422 | 417 |
| 3E | 28 | 450 | 420 |
| 3D | 28 | 448 | 418 |

in the center as a result of internal heating from deposition of gamma rays. Temperatures for the various positions are reported in Table 3.2. Standard shear punch specimens from a similar block not irradiated in the reactor were also provided. Because of limited material availability, only three specimens were tested for each position within the blocks.

### 3.4.2 Test Area

The testing facility was modified to accommodate testing of the irradiated materials in a lightly controlled area. Specimen loading was done in a fume hood to control dispersement of any potential contaminants. The shear punch fixture was suitable for trapping any contaminants formed during testing by placing a piece of tape on the bottom of the receiving die. This was necessary to minimize potential contamination to the Instron test frame as the hole in which the shear punch specimen deforms is located through the entire thickness of the receiving die. It was shown before testing that the effect of the tape had a minimal effect on mechanical strength measurements.

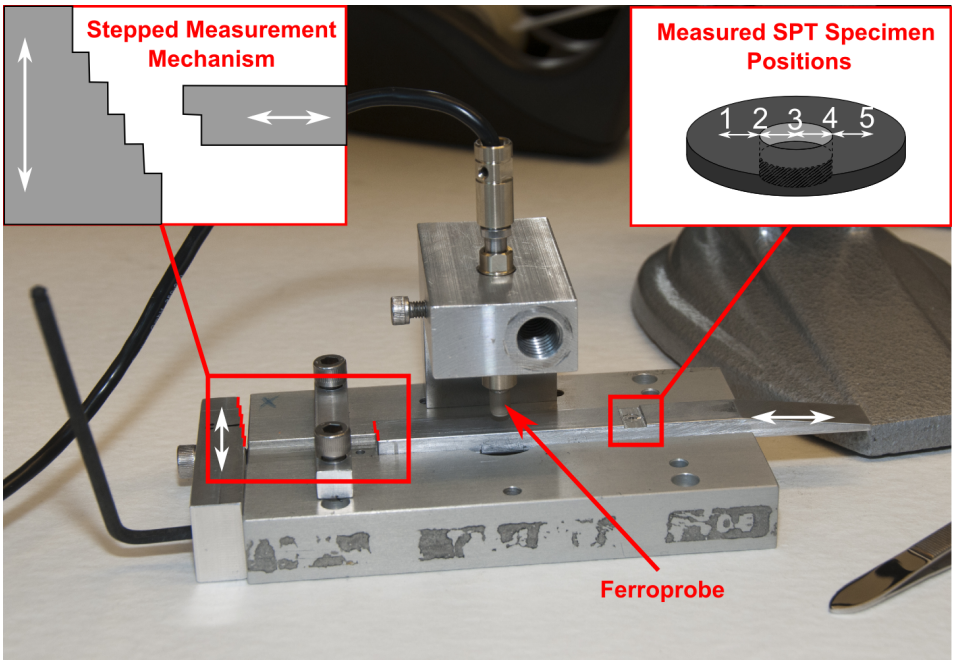


**Figure 3.7:** Image and schematic of ferroprobe alignment tool.

## 3.5 Detecting Strain-Induced Martensitic Transformations through Ferromagnetic Measurements

Changes in ferromagnetism due to strain-induced martensitic transformations in 304SS were measured using a commercial Fisher FMP30 Ferritescope. A tool was developed to allow for precise measurements on an SPT specimen. A schematic of the tool is shown in Figure 3.7. A movable "stepped measurement mechanism" (defined in Figure 3.7) allowed measurements of five areas across the specimen width at 0.5 mm intervals: corresponding to two positions in the undeformed bulk region (labeled 1 and 5 in Figure 3.7), two positions on either edge of the deformed region (labeled 2 and 4), and one position in the center of the punched region (labeled 3). Specimens were aligned with respect to the punched region of the SPT specimen after testing.

# 4 RESULTS AND DISCUSSION

## 4.1 Determination of Shear Yield Stress and Tensile/Shear Correlations

Correlations between the miniature tensile and shear punch techniques were accomplished by comparing experimentally obtained strengths measured through the two test techniques. This correlation was done by finding the linear fit of the data defining an intercept through (0,0). Figure 4.1 (a) shows comparisons of ultimate strength obtained through the shear punch test with the strength obtained using the miniature tensile technique. A linear correlation of $\sigma_{ult,tensile} = 1.4\tau_{ult,shear}$ was observed. This value is similar to the tensile-to-shear ultimate strength ratio of $1.29 - 2.049$ reported in literature [2, 5–7, 9]. A comparison to the ratio measured in this research to reported tensile/shear ratios is shown in Figure 4.1 (b) and Table 4.1.

Yield strength correlations were made by comparing experimentally obtained yield strengths determined using the strain offset method. For tensile experiments, yield stress is calculated using the standard $0.2\%$ offset. As there is not a standardized strain offset

**Table 4.1:** Comparison of tensile/shear ultimate stress ratios reported in literature and this research.

| Reference | $\sigma_{ult}/\tau_{ult}$ |
|---|---|
| Guduru, *et al.* [2] | 1.8 |
| Karthik, *et al.* [5] | 2.042 |
| Karthik, *et al.* [6] | 1.29 |
| Toloczko, *et al.* [9] | 1.31 |
| This work | 1.4 |

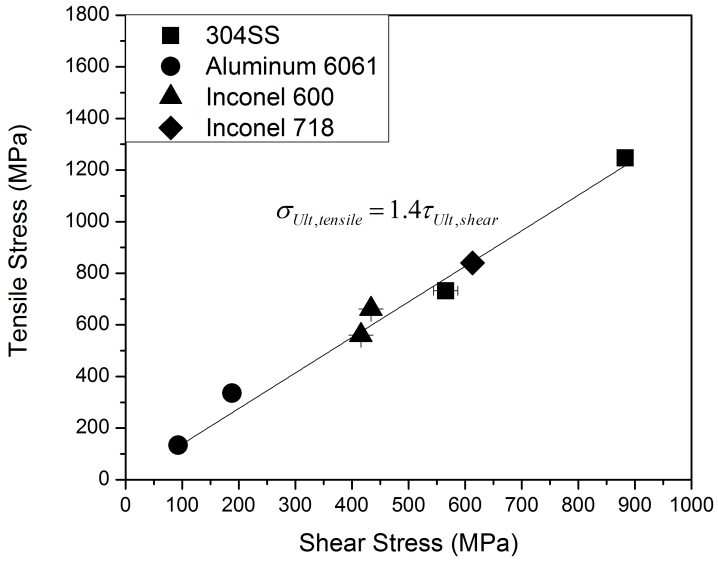


**(a)**

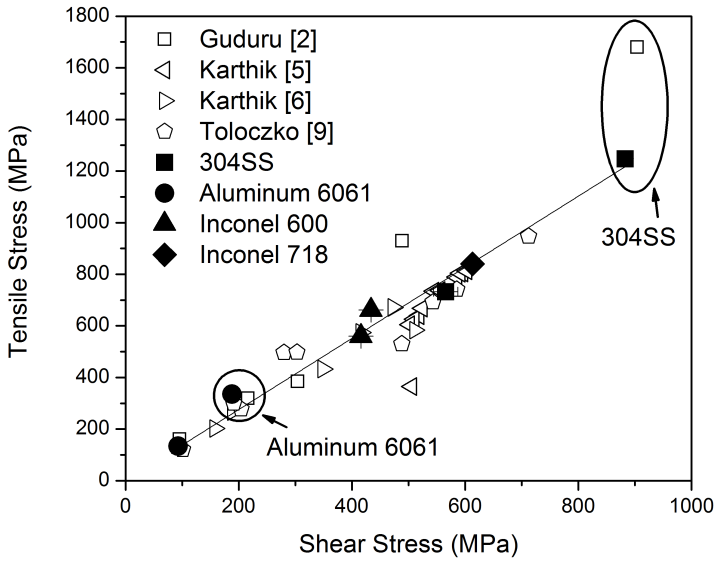


**(b)**

**Figure 4.1:** Comparisons of ultimate strength obtained through the shear punch and miniature tensile techniques. (a) shows the data measured in these experiments. (b) compares the strength measured in these experiments to those reported in literature where the circled points note comparisons of the tensile/shear ratios of either 304SS or aluminum 6061 measured in this research to those reported in literature.

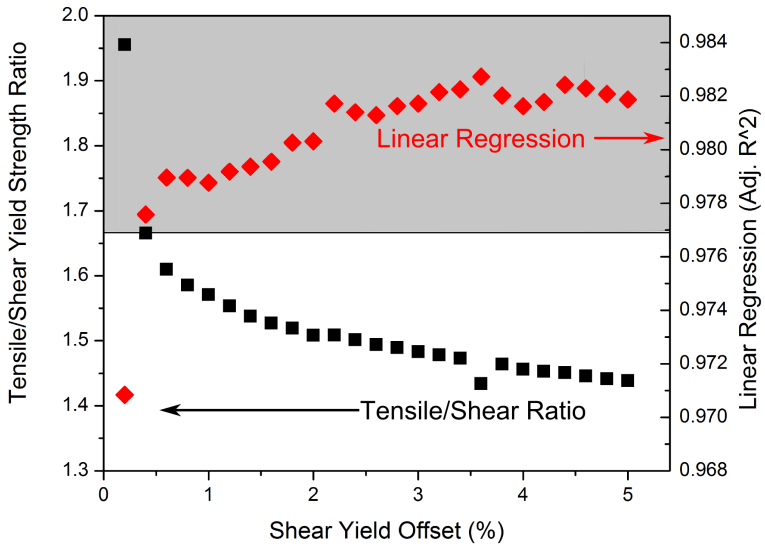


**Figure 4.2:** Tensile/shear ratio calculated through comparisons of shear yield stress calculated using offsets between $0.2\%$ and $5\%$ and compared to tensile yield information measured using a standard $0.2\%$ offset. The shaded region corresponds to the range of tensile/shear ratios that have been reported in [2–10]. Linear regression of the line fit was included to show the offset that provided the best fit.

used to determine shear yield stress, this value had to be established before the tensile/shear correlation was made.

To establish the shear yield offset, yield stress was calculated for strain offsets between $0.2\%$ and $5\%$ at $0.2\%$ intervals. The set of stresses calculated for each offset were individually compared to tensile yield stresses measured using $0.2\%$ strain offset. Figure 4.2 shows the calculated tensile/shear yield stress ratio, as well as the linear regression of the fit. The shaded region represents the tensile/shear yield stress ratios between 1.67 and 2.3 reported in literature [2–10].

**Table 4.2:** Shear yield stress calculated using the $0.2\%$ and $1\%$ offsets typically used in literature with the $2.2\%$ offset used in this study.

| | | Shear yield stress (MPa) measured using: | | |
|---|---|---|---|---|
| Material | Treated Condition | $0.2\%$ Offset | $1\%$ Offset | $2.2\%$ Offset |
| 304SS | Annealed | $161 \pm 39$ | $182 \pm 36$ | $202 \pm 34$ |
| | Treated | $553 \pm 44$ | $608 \pm 22$ | $639 \pm 13$ |
| Aluminum 6061 | T0 | $57 \pm 13$ | $60 \pm 11$ | $64 \pm 9$ |
| | T6 | $130 \pm 12$ | $146 \pm 8$ | $157 \pm 5$ |
| Inconel 600 | Annealed | $96 \pm 22$ | $120 \pm 14$ | $145 \pm 11$ |
| | Solution Treated | $81 \pm 30$ | $97 \pm 26$ | $118 \pm 20$ |
| Inconel 718 | Annealed | $188 \pm 73$ | $254 \pm 8$ | $286 \pm 8$ |
| | Aged | $510 \pm 5$ | $584 \pm 5$ | $633 \pm 5$ |

Figure 4.2 shows a comparison of the tensile/shear yield strength ratio measured using strain offsets between $0.2\%$ and $5\%$. Highlighted in the figure is the range of tensile/shear yield strength ratios reported in literature for easy comparisons. These measured yield strength ratios are compared to the linear regression for the calculated slopes. While the $3.6\%$ offset showed the least deviation from linearity (highest linear regression), this offset was not chosen for two reasons. First, this offset showed the highest deviation from the tensile/shear yield strength ratio range reported in litereature. Second, shear yield strength measurements using this high offset may not be representative of yielding as it can be well into the plastic deformation region of the stress-strain curve.

The shear strain offset of $2.2\%$ provided a relatively low deviation from linearity while also measuring closer to deviation from the elastic linear region of the stress-strain curve. The tensile/shear yield ratio calculated using the $2.2\%$ shear strain offset provided a better linear regression as compared to the standard $0.2\%$ and $1\%$ offsets. Additionally, there was less error measured for the shear yield stress measured for each material using the $2.2\%$ strain offset compared to the $0.2\%$ and $1\%$ offsets, shown in Table 4.2.

**Table 4.3:** Comparison of tensile/shear yield strength ratios reported in literature and this work.

| Reference | $\sigma_y/\tau_y$ |
|---|---|
| Guduru, *et al.* [2] | 1.77 |
| Guduru, *et al.* [3] | 1.773 |
| Karthik, *et al.* [5] | 2.093 |
| Karthik, *et al.* [6] | 1.73 |
| Toloczko, *et al.* [9] | 1.67 |
| This work | 1.5 |

Figure 4.3 (a) shows the tensile/shear yield strength correlation using the $2.2\%$ shear yield offset which correponded to a $\sigma_{y,tensile\ (0.2\%\ offset)} = 1.5\tau_{y,shear(2.2\%\ offset)}$. This value is a bit lower than the $1.67 - 2.3$ range reported in literature [2, 5–7, 9] and 1.73 ratio derived using the Von Mises yield criterion [18], shown in Figure 4.3 (b) and Table 4.3. This variance might be explained if the shear punch specimen is not stressed in pure shear.

## 4.2 Effect of Surface Roughness on Shear Strengths

A limited number of studies have noted that surface roughness does not appear to impact the strength measured by shear punch experiments [2]. Because the valuable irradiated specimens obtained for determining irradiation effects were received in a rough polished surface finish, the effect of surface roughness was re-visited. The material used for determining the effect of surface finish was an annealed 304SS, a similar grade to the material tested in the irradiation tests. The effect of surface roughness was also studied for miniature tensile experiments to further develop the technique.

Figure 4.4 shows how miniature tensile mechanical strength varies with surface roughness. Statistically insignificant differences (using a one-way ANOVA, Tukey means comparison) were observed in both yield and ultimate strengths for the surface roughnesses tested.

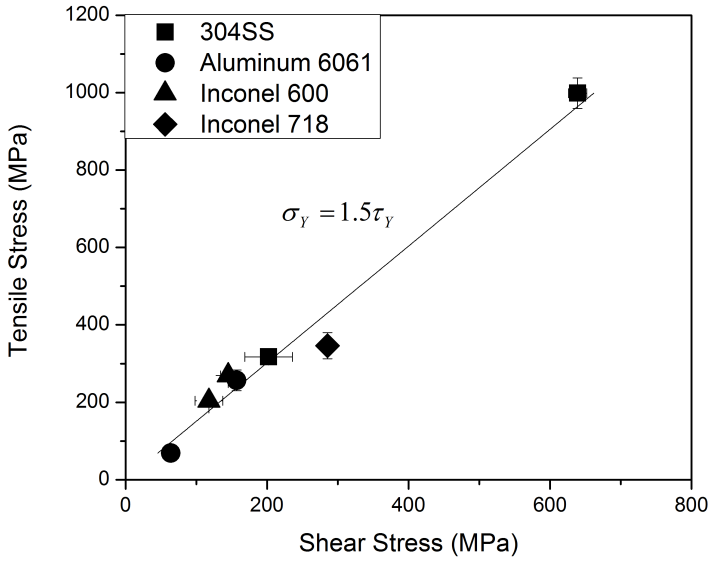


**(a)**

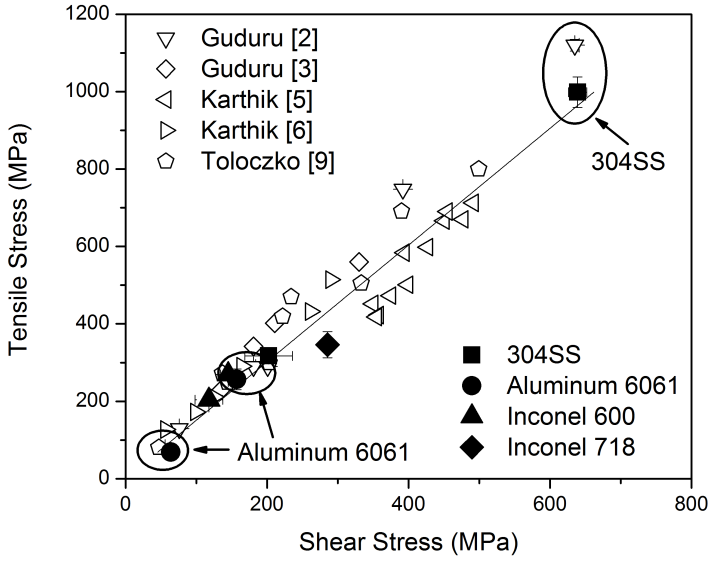


**(b)**

**Figure 4.3:** Comparisons of yield strength obtained through the shear punch and miniature tensile techniques. (a) shows the data measured in these experiments. (b) compares the strength measured in these experiments to those reported in literature where the circled points note comparisons of the tensile/shear ratios of either 304SS or aluminum 6061 measured in this research to those reported in literature.

Figure 4.5 shows how shear punch mechanical strength varies with surface roughness. Statistically insignificant differences (using a one-way ANOVA, Tukey means comparison) were observed in both yield and ultimate strengths for various surface roughnesses ranging from a relatively rough 600 SiC grit to a smooth $0.5\ \mu m$ diamond paste polishes. This finding is similar to those reported by [2], where the specimens were not sensitive to the 600 grit and 2400 grit tested.

The insignificant differences in strength with various surface finishing ranging from "rough" to "smooth" suggest that the surface layer damaged from the polishing process is minimal as compared to the specimen thickness. For both the miniature tensile and shear punch experiments, this study shows that surface finish will not affect measured strength. This knowledge reduces specimen preparation time and gives confidence that varying surface roughness between specimens will not convolute analysis in the study of irradiation effects, as discussed in Sections 4.4 through 4.6.

### 4.3 Effect of Specimen Thickness on Stress-Strain Curves

The effect of specimen thickness on both the shear punch and miniature tensile tests were studied mainly to determine the minimum specimen thickness required to obtain accurate data, particularly when studying the impact of irradiation effects on strength properties. Aluminum 6064 T6 treated material was chosen for this study as the low strength provided the best opportunity to observe variations in strength based on specimen thickness.

Additionally, correlations in ductility with specimen thickness were investigated for the two mechanical test techniques. Understanding how ductility is affected with specimen thickness may be helpful as an initial detection of martensitic transformations. In reported studies, some strain-induced martensitic transformations in irradiated materials were initially

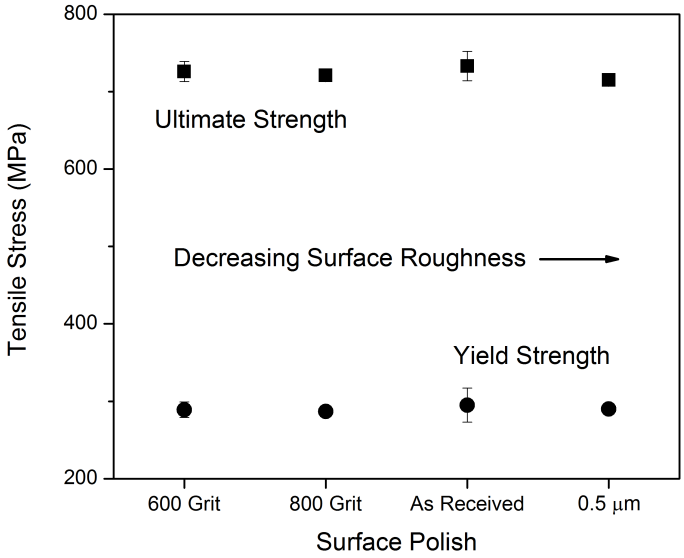


**Figure 4.4:** Effect of surface roughness on strength obtained through the miniature tensile technique with surface defects introduced through grinding and polishing.

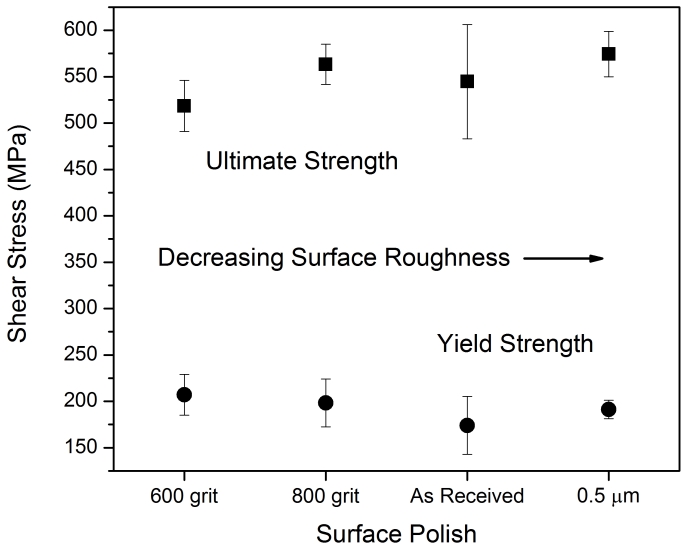


**Figure 4.5:** Effect of surface roughness on strength obtained through shear punch testing with surface defects introduced through grinding and polishing procedures.

detected by abnormal increases in ductility [17, 21–23]. The ability to correlate ductility with specimen thickness would help suggest whether unusual differences in overall ductility refer to martensite formed during mechanical testing or note variations in specimen thickness.

### 4.3.1 Thickness Effects on Shear Punch Experiments

Figure 4.6 (b) shows how yield and ultimate strengths vary with specimen thickness for the shear punch test. A statistically significant difference (one-way ANOVA, Tukey means comparison) was observed for the $100\ \mu m$ thickness when compared to the $200$ through $300\ \mu m$ thicknesses. No statistically significant difference was observed in ultimate strength with varying thickness. Another characteristic of Figure 4.6 (b) is the increased error ($\pm 1$ standard deviation of data set) for the $100$ and $150\ \mu m$ thick specimens. This suggests that $200\ \mu m$ is the minimum specimen thickness required for shear punch experiments to obtain accurate strength data.

Figure 4.6 (a) shows how the maximum strain until failure varies with thickness for shear punch experiments. A larger variation in elongation was observed for $100\ \mu m$ thick specimens as compared $150$ through $300\ \mu m$ thicknesses. Additionally, there was a decreasing trend in maximum strain before failure as specimen thickness increased, though there was no statistical difference between the $150$ through $300\ \mu m$ thick specimens. Similar to comparisons of varying specimen thickness and strength, approximately $200\ \mu m$ thick specimens are required to avoid major differences in maximum elongation.

These results suggest that specimens between $200$ and $300\ \mu m$ thick minimally affect strength and maximum elongation obtained through shear punch experiments. This allows confidence in strength measurements with variations in specimen thickness. Additionally, large abnormalities in ductility for specimens within this thickness range can be attributed

to factors other than varying specimen thickness, such as the formation of martensite in irradiated steels.

### 4.3.2 Tensile Thickness Effects on Character of Stress-Strain Curves

Figure 4.7 (a) shows how the maximum strain to failure varies with thickness for miniature tensile experiments. For the tested thickness range, a significant difference in elongation is observed. With the thicker specimens, the larger amount of material within the specimen cross-section resists dislocation movement until the specimen fails brittlely. For the thinner specimens, less material is available and there are a lower number of obstacles restricting how the material deforms. This allows the thinner specimens to stretch more than the thicker specimens resulting in a decrease in ductility with increasing specimen thickness for miniature tensile experiments.

Figure 4.7 (b) shows how ultimate and yield strength vary with specimen thickness for aluminum 6061, T6 treated miniature tensile experiments. A statistical difference was observed for ultimate strength (see inset of 4.7 (b)), though the difference between the values was less than 10 MPa, a minimal difference as compared to the overall strength. Additionally, no variations were observed in ultimate strength with increasing specimen thickness.

A different observation was seen for the tensile yield strength. A much lower yield strength was observed for the 0.8 mm thickness than the 1 mm or 1.2 mm thickness specimens: approximately 100 MPa was measured for the 0.8 mm thick specimens as compared to approximately 250 MPa for 1 mm and 1.2 mm thick specimens. While this might suggest a threshold thickness of 1 mm is required for the aluminum 6061, T6 treated material, further inspection of the specimen surface that was in contact with the grips of the tensile fixture

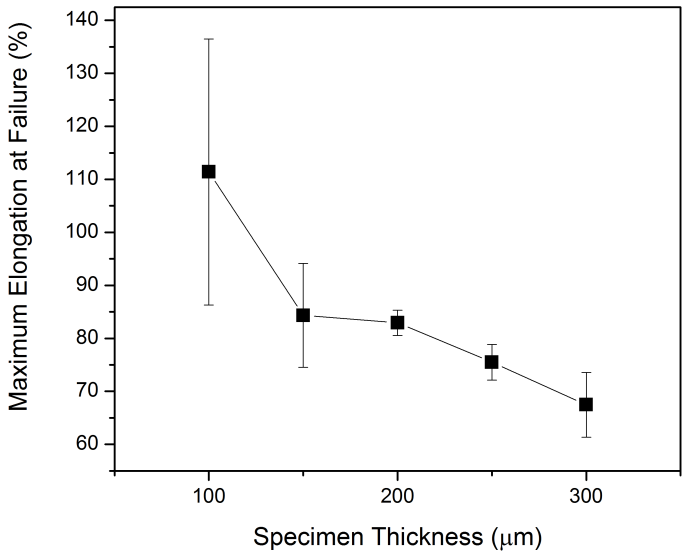


**(a)**

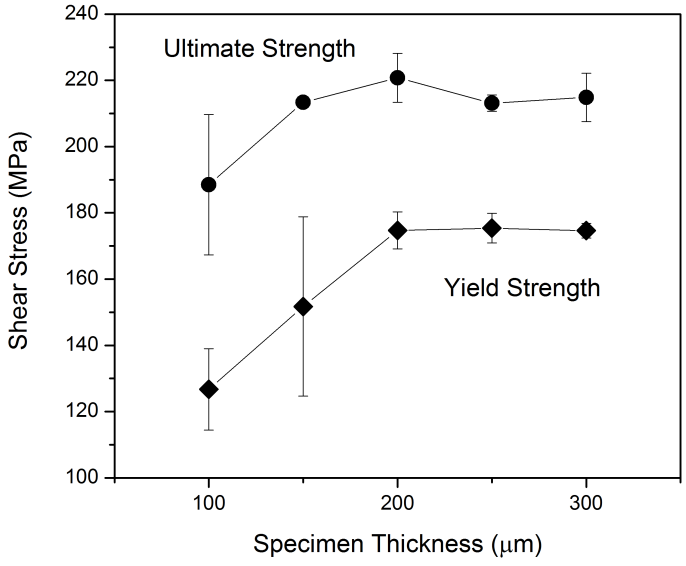


**(b)**

**Figure 4.6:** (a) Maximum strain at failure and (b) yield and ultimate strength for aluminum 6061, T6 treated SPT specimens with thicknesses between $100$ and $300$ $\mu m$.

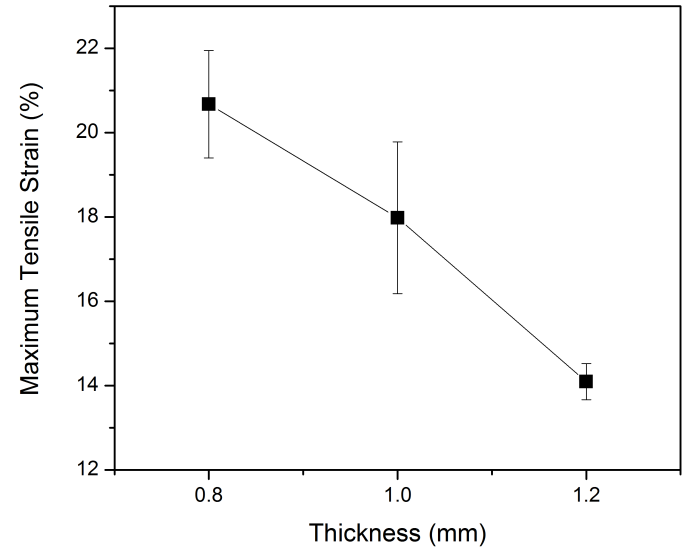


**(a)**

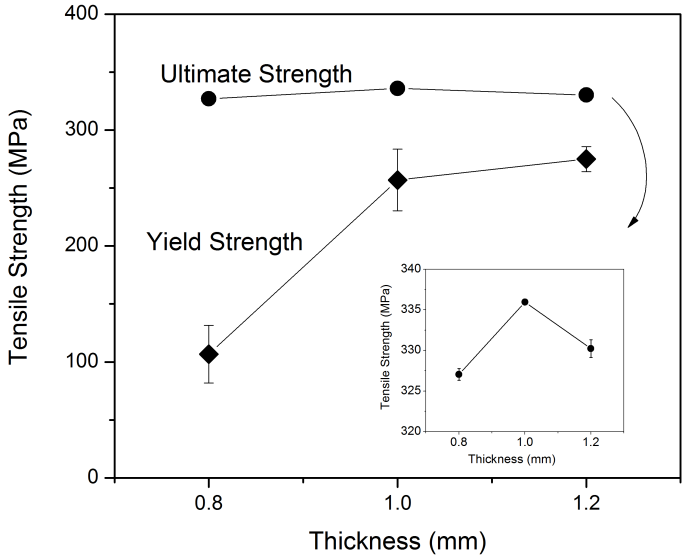


**(b)**

**Figure 4.7:** (a) Maximum strain at failure and (b) yield and ultimate strength for aluminum 6061, T6 treated miniature tensile specimens with thickness varying between $100$ and $300$ $\mu m$.

suggest the 0.8 mm thick specimens may have reseated during testing, affecting the character of the stress-strain curves.

Figure 4.8 shows the surface of two of the 0.8 mm thick specimens as well as the surface of one 1 mm and 1.2 mm thick specimen. Comparing the divots formed from gripping the specimen in the test fixture (circled in Figure 4.8), it appears some reseating may have occurred in the lower grip for the 0.8 mm thick specimens. In the 0.8 mm thick specimens, a "smeared" divot with a large surface area is observed while the 1 mm and 1.2 mm thick specimens have a more "pinpoint" appearance with a smaller divot area. Further inspection of the individual curves for the four 0.8 mm thick specimens tested also shows this effect where a lower divot area corresponds to a higher measured yield stress.

Comparing the images of specimens labeled MT208 (Figure 4.8 (a) and (e)) and MT211 (Figure 4.8 (b) and (f)) and the individual stress-strain curve behavior for the specimens in Figure 4.9, the larger slip area in MT208 corresponds to a lower yield stress. This variation suggests that if the specimens were held correctly within the grips and no reseating occurred, a similar yield stress would have been observed for the 0.8 mm thick specimens as the 1 mm and 1.2 mm thick specimens. Then the data might have shown that the 0.8 mm thick specimens would obtain repeatable data.

### 4.4 Effect of Irradiation Damage on Mechanical Properties

With the confidence in the shear punch test as discussed in Sections 4.1 through 4.3, irradiation effects were studied using this testing technique. Figure 4.10 shows how yield and ultimate strength varied with dose. Typically an increase in strength was observed, saturating at relatively low doses. This finding is consistent to observations reported in literature [26, 30] where yield and ultimate strength saturate at approximately 10 dpa.

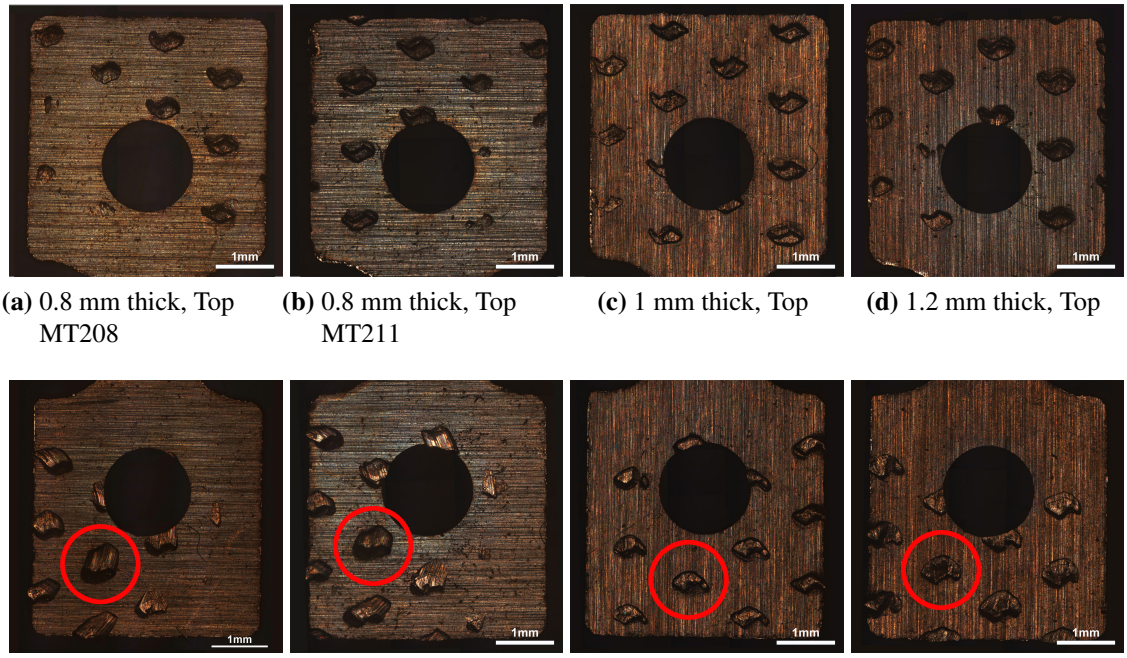


**(a)** 0.8 mm thick, Top MT208 **(b)** 0.8 mm thick, Top MT211 **(c)** 1 mm thick, Top **(d)** 1.2 mm thick, Top

**(e)** 0.8 mm thick, Bottom MT208 **(f)** 0.8 mm thick, Bottom MT211 **(g)** 1 mm thick, Bottom **(h)** 1.2 mm thick, Bottom

**Figure 4.8:** Upper and lower grips of two 0.8 mm thick, one 1 mm thick, and one 1.2 mm thick miniature tensile specimens after miniature tensile testing. A decreasing grip mark area (circled on the lower grip positions) was noticed for an increasing specimen thickness, corresponding to an increasing yield strength shown in Figure 4.9. For the two 0.8 mm thick specimens, the specimen labeled MT208 showed a larger grip smear area (circled in (e)), which corresponded to a lower measured yield strength. For the specimen labeled MT211, which was also 0.8 mm thick, a lower amount of smearing was observed (circled in (f)), which corresponded to a higher measured yield strength as compared to MT208.

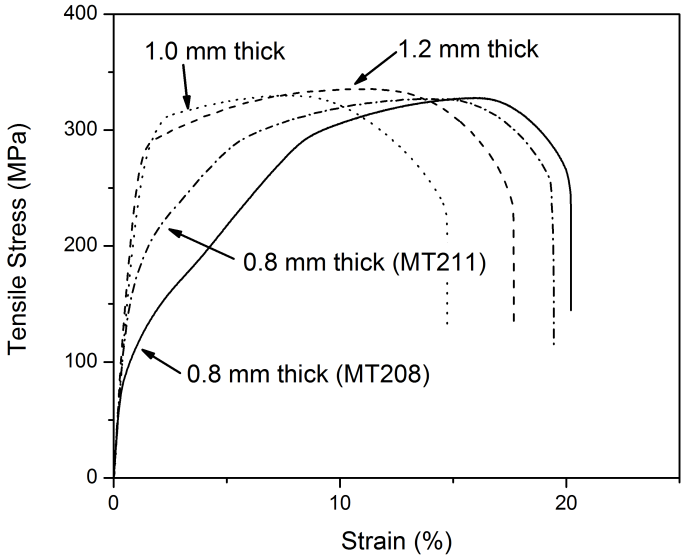


**Figure 4.9:** Stress-strain curve behavior for four aluminum 6061, T6 treated miniature tensile specimens tested with 0.8, 1.0, and 1.2 mm thicknesses. A higher yield strength was observed for the 1.0 and 1.2 mm thick specimens as compared to the two 0.8 mm thick specimens shown in Figure 4.8. For the two 0.8 mm thick specimens, the one with a higher yield stress (MT211) corresponded to lower observed slipping on the grip sections shown in Figure 4.8.

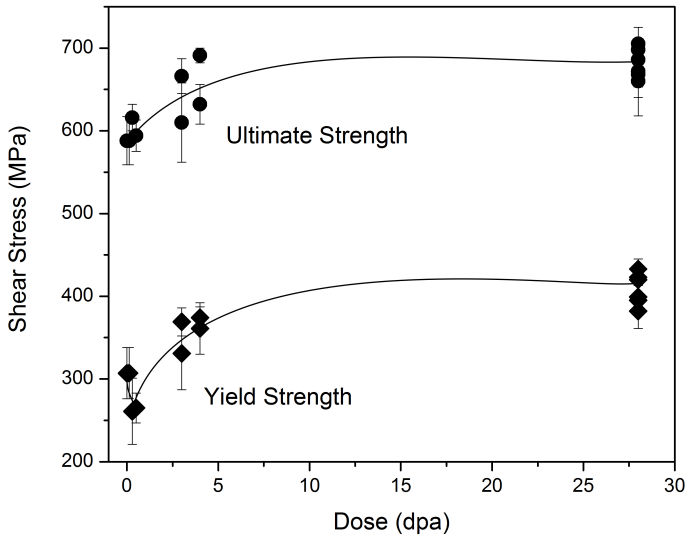


**Figure 4.10:** Yield and ultimate strengths obtained through the shear punch test with varying irradiation exposures where a saturation in strength is observed when moving from the unirradiated condition to high doses.

A closer examination of strength from the low dose region, shown in Figure 4.11, shows an initial decrease in measured yield strength when moving from the non-irradiated to a low ($< 1$ dpa) irradiation exposure conditions. While any irradiation damage on annealed material would result in the formation of defects that impede dislocation motion, subsequent examination by electron microscopy indicated the material tested had a dislocation density consistent with about $5\%$ residual cold-work. Therefore, the drop in yield strength from the unirradiated to doses less than 1 dpa is speculated to be from a reduction in dislocation density with irradiation. This finding is consistent with observations from other studies [26].

### 4.5 Effect of Irradiation Temperature on Mechanical Properties

The effect of irradiation temperature on strength was also evaluated for material exposed to 28 dpa. The variation in temperature was approximately $40$ °C. Figure 4.12 shows

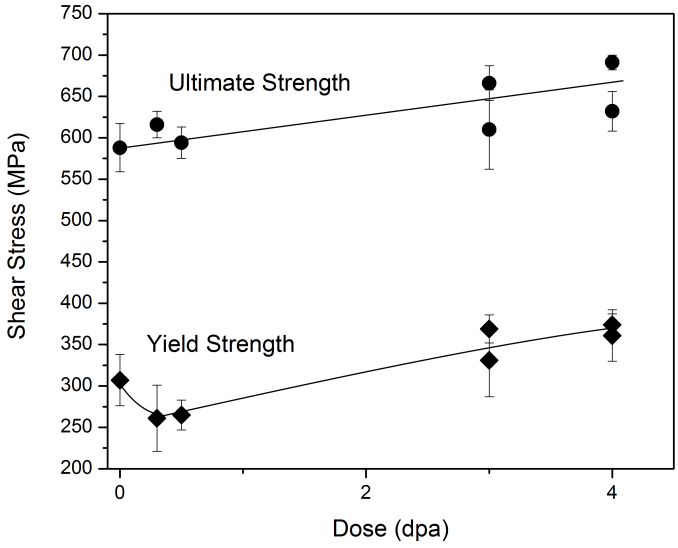


**Figure 4.11:** A closer look of Figure 4.12 where the shear punch yield and ultimate strengths is shown for low doses showing initial decrease in strength for the 0.3 dpa dose compared to the unirradiated condition.

a decreasing trend in strength with temperature. One explanation for this trend is some annealing occurred at the higher temperatures.

Another explanation for the observed decreases in strength with increasing temperature could be due to higher defect motion at higher temperatures. The greater defect motion gives a higher probability of defect interactions leading to defect annihilation. If some defects annihilate, a lower number of obstacles remain to resist dislocation motion and lead to a decrease in strength.

### 4.6 Effect of Strain-Induced Martensitic Transformations

While the main goal of testing the irradiated hex block material was to observe how varying radiation dose and temperature levels affect mechanical strength of 304SS, another factor that might affect strength are phase transformations induced from the shear punch

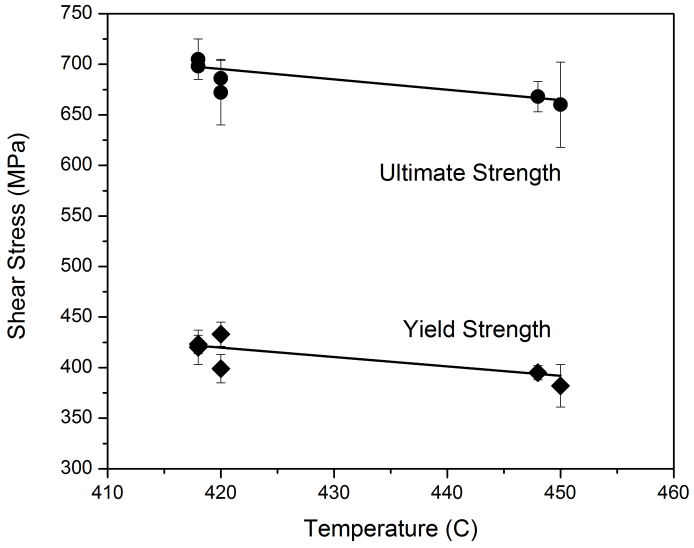


**Figure 4.12:** Shear punch yield and ultimate strengths showing a decreasing trend in strength with increasing irradiation temperature for material exposed to 28 dpa.

technique itself. The 304SS austenitic stainless steel tested has been shown to be susceptible to strain-induced martensitic transformations [17, 21–24]. As the transformed martensite phase is ferromagnetic, it is possible to detect how much material was transformed in tensile specimens using a ferroprobe [17].

A Fisher FMP-30 Feritescope was used to measure ferromagnetic content where ferromagnetism was reported in ferrite number (FN). The probe consists of a handset and probe similar to a pencil, as shown in 4.13. A series of measurements were made across the SPT specimen width both before and after SPT in order to detect a relative change in FN values.

A fixture was developed to allow precise measurements across the width of the shear punch specimen. The fixture, shown in Figure 4.14 (a), consists of the alignment of a punched SPT specimen with respect to the punched region on a movable slide. The slide rests along a stepped measurement stop in which ferroprobe measurements correspond to five different


**Figure 4.13:** Fisher FMP-30 Feritescope, consisting of a handset and pencil-like probe

positions along the width of the SPT specimen: two undeformed regions (marked 1 and 5 on Figure 4.14 (a)), two on the edge of the punched region (directly above deformed material, marked 2 and 4), and one in the center of the punched region.

Figure 4.14 (b) shows the ferroprobe measurement at five positions along the width of three shear punch specimens in the 0.5 dpa set both before and after SPT. The figure shows a repeatable FN for the sample set across the specimen width. There are two interesting characteristics in the readings; the first being an increased reading in the unpunched region (marked 1 and 5 in Figure 4.14 (a)) after shear punch as compared to before testing. It was assumed that deformation only occurred along the edge of the punched region. The heightened FN reading in the non-deformed region of the specimen may be due to a large interaction volume of the ferroprobe. This finding suggests that some martensite may have formed during shear testing, indicated by the increase in FN before and after testing. Work is in progress to confirm the presence of martensite through transmission electron microscopy

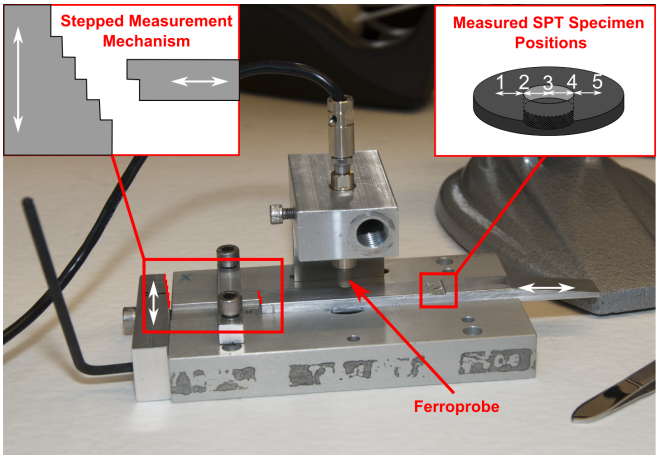


**(a)**

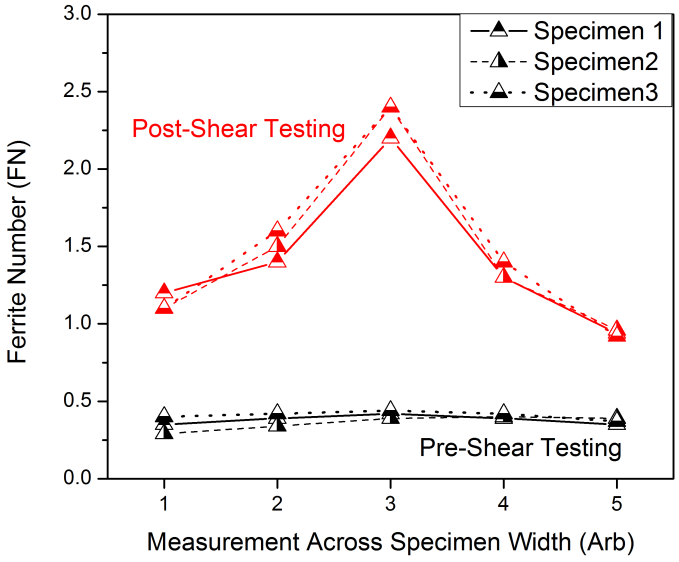


**(b)**

**Figure 4.14:** (a) Review of fixturing used to detect ferromagnetic changes on shear punch specimens as described in Section 3.5. (b) Comparison of ferrite numbers before and after shear testing showing reproducibility in measurement technique for three specimens in the 0.5 dpa set. The measurement across specimen surface corresponds to the positions on the specimen surface noted in (a).

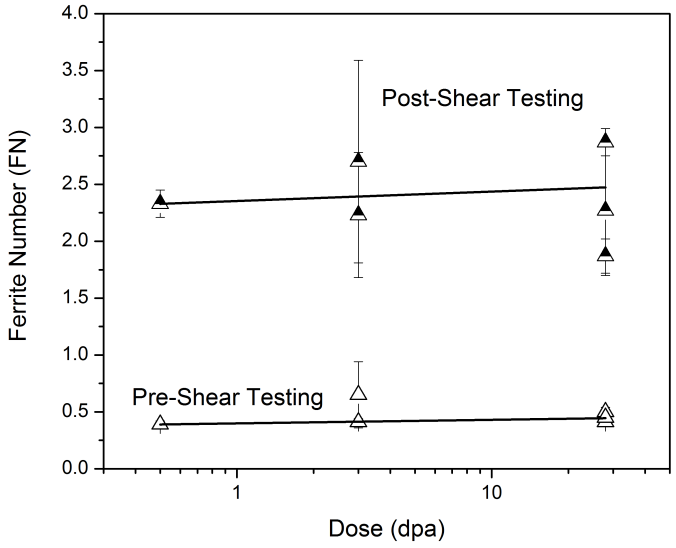


**Figure 4.15:** Comparison of changes in ferrite number measurements before and after shear testing with respect to dose.

(TEM), though is not part of the scope of this thesis due to issues associated with preparing radioactive samples.

Another other interesting characteristic observed in Figure 4.14 (b) was the increased reading in the center of the punched region as compared to the "ring" measurement directly above the deformed region in the specimen. Since the flat punched portion was not deformed during testing, the increase in readings are likely due to increased contact between the sides of the probe and the deformed edge. Because of the increased contact, only measurements from this center position are reported.

The changes in FN before and after shear testing for all doses is shown in Figure 4.15. All doses showed similar FN readings prior to shear testing. An increase in FN was observed for each dose after shear testing. These increases were typically similar with respect to dose, though a larger scatter was observed as dose increased.

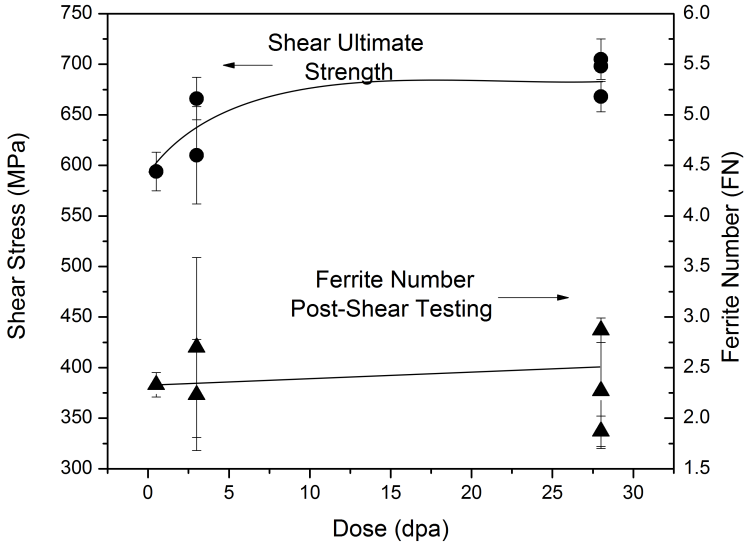


**Figure 4.16:** Comparison of the measured shear ultimate strength and ferrite number with respect to irradiation dose.

Comparing the FN measurements to the shear ultimate strengths for the irradiated hex blocks, as shown in Figure 4.16, it appears the strain-induced martensitic transformations have a minimal effect on material strength. For each dose, approximately the same change in ferromagnetism was observed before shear punch testing while the strength was observed to increase with increasing dose.

# 5 CONCLUSIONS

Property-property correlations were made on unirradiated material between shear punch and standard miniature tensile techniques. To ensure the reliability of the shear punch test, the effect of surface roughness and specimen thickness on measured strength was investigated. These experiments showed that surface roughness has no effect on strength. It was demonstrated that for aluminum 6061, the softest of the materials tested, strength was minimally affected by strength above $200\ \mu m$.

The resulting tensile/shear yield strength correlation was shown to be 1.5, on the lower end of the correlation of 1.67 - 2.3 [2–10] reported in literature. The tensile/shear ultimate strength correlation was shown to be 1.4, similar to published data where the trend has been reported as between 1.29 - 2.042 [2, 5–7, 9].

Based on the standardization of the shear punch test, this technique was applied to material irradiated to 0.3-28 dpa. The following was noticed for the shear punch experiments:

1. Good reproducibility between data sets.

2. Shear punch experiments showed the same tendencies with respect to hardening, as shown in many other studies using tensile experiments.

3. Tendency for yield and elongation to saturate early in irradiation strength parameters and also shown to fall with temperature, as noted in other studies.

To determine whether the observed hardening was affected by the formation of martensite during shear punch testing, a non-destructive technique was developed to observe changes in

ferromagnetism that are characteristic of a martensitic transformation. It was shown that there was a tendency to form martensite at low dpa values. Based on these studies it would appear the strength of the irradiated steel tested saturates at a shear yield strength of approximately 400 MPa and a shear ultimate strength of 670 MPa.

# REFERENCES

[1] *ASTM Standard E 8M-04, 2005* "Standard test methods for tension testing of metallic materials [metric]" , ASTM International, West Conshohocken, PA, 2005.

[2] R. K. Guduru, K. A. Darling, R. Kishore, C. C. Koch, and K. L. Murty, "Evaluation of mechanical properties using shear-punch testing," *Mater. Sci. Eng. A Struct. Mater.*, **395** [1-2] 307–314 (2005).

[3] R. Guduru, R. Scattergood, C. Koch, K. Murty, and A. Nagasekhar, "Finite element analysis of a shear punch test," *Metall. Mater. Trans. A*, **37** 1477–1483 (2006).

[4] G. L. Hankin, M. B. Toloczko, K. I. Johnson, M. A. Khaleel, M. L. Hamilton, F. A. Garner, R. W. Davies, and R. G. Faulkner, "An investigation into the origin and nature of the slope and x-axis intercept of the shear punch-tensile yield strength correlation using finite element analysis," *ASTM STP 1366*, 1018–1028 (2000).

[5] V. Karthik, K. Laha, P. Parameswaran, K. V. Kasiviswanathan, and B. Raj, "Small specimen test techniques for estimating the tensile property degradation of mod 9Cr-1Mo steel on thermal aging," *J. Test. Eval.*, **35** [4] 1–11 (2007).

[6] V. Karthik, P. Visweswaran, A. Vijayraghavan, K. V. Kasiviswanathan, and B. Raj, "Tensile shear correlations obtained from shear punch test technique using a modified experimental approach," *J. Nucl. Mater.*, **393** [3] 425 – 432 (2009).

[7] G. E. Lucas, J. W. Sheckherd, G. R. Odette, and S. Panchanadeeswaran, "Shear punch tests for mechanical property measurements in TEM disc-sized specimens," *J. Nucl. Mater.*, **122-123** 429–434 (1984).

[8] M. B. Toloczko, R. J. Kurtz, A. Hasegawa, and K. Abe, "Shear punch tests performed using a new low compliance test fixture," *J. Nucl. Mater.*, **307-311** 1619–1623 (2002).

[9] M. B. Toloczko, R. J. Kurtz, K. Abe, and A. Hasegawa, "Tensile property estimates obtained using a low compliance shear punch test fixture," *ASTM STP 1447*, 612–622 (2004).

[10] M. B. Toloczko, K. Abe, M. L. Hamilton, F. A. Garner, and R. J. Kurtz, "The effect of test machine compliance on the measured shear punch yield stress as predicted using finite element analysis," *ASTM STP 1418*, **4** 339 – 349 (2002).

[11] G. L. Hankin, M. B. Toloczko, M. L. Hamilton, and R. G. Faulkner, "Validation of the shear punch-tensile correlation technique using irradiated materials," *J. Nucl. Mater.*, **258-263** 1651–1656 (1998).

[12] G. E. Lucas, "The development of small specimen mechanical test techniques," *J. Nucl. Mater.*, **117** 327–339 (1983).

[13] D. A. Smith and R. Bakerjian, *Die Design Handbook*, 3rd edition; pp. 4.1–4.32, Society of Manufacturing Engineers, Dearborn, MI, 1990.

[14] M. B. Toloczko, M. L. Hamilton, and G. E. Lucas, "Ductility correlations between shear punch and uniaxial tensile test data," *J. Nucl. Mater.*, **283-287** 987–991 (2000).

[15] M. B. Toloczko, M. L. H. Y. Yokokura, K. Abe, F. A. Garner, and R. J. Kurtz, "The effect of specimen thickness and grainsize on mechanical properties obtained from the shear punch test," *ASTM STP 1418*, **4** 371–379 (2002).

[16] R. K. Guduru, A. V. Nagasekhar, R. O. Scattergood, C. C. Koch, and K. L. Murty, "Thickness and clearance effects in shear punch testing," *Adv. Eng. Mater.*, **9** [3] 157–160 (2007).

[17] M. N. Gusev, O. P. Maksimkin, and F. A. Garner, "Peculiarities of plastic flow involving "deformation waves" observed during low-temperature tensile tests of highly irradiated 12Cr18Ni10Ti and 08Cr16Ni11Mo3 steels," *J. Nucl. Mater.*, **403** 121–125 (2010).

[18] J. Roesler, H. Harders, and M. Baeker, *Mechanical Behaviour of Engineering Materials: Metals, Ceramics, Polymers, and Composites*; pp. 63–118, Springer, Berlin, NY, 2007.

[19] R. W. Hertzberg, *Deformation and Fracture Mechanics of Engineering Materials*; pp. 3–56, John Wiley & Sons, Inc., New York, 1996.

[20] G. S. Was, *Fundamentals of Radiation Materials Science*; pp. 581–642, Springer, Berlin, 2007.

[21] M. N. Gusev, O. P. Maksimkin, I. S. Osipov, and F. A. Garner, "Anomalously large deformation of 12Cr18Ni10Ti austenitic steel irradiated to 55dpa at 310C in the BN-350 reactor," *J. Nucl. Mater.*, **386-388** 273–276 (2009).

[22] M. N. Gusev, D. A. Toktogulova, O. P. Maksimkin, and F. A. Garner, "A new deformation mode observed in austenitic low-nickel stainless steels irradiated to high

neutron exposure at 310-432C"; pp. 1385–1391 *14th Int. Conf. on Environmental Degradation of Materials in Nuclear Power Systems*.

[23] M. N. Gusev, O. P. Maksimkin, I. S. Osipov, N. S. Silniagina, and F. A. Garner, "Unusual enhancement of ductility observed during evolution of a "deformation wave" in 12Cr18Ni10Ti stainless steel irradiated in BN-350," *J. ASTM Int.*, **6** [7] 1–7 (2009).

[24] P. L. M. Jr. and G. Thomas, "The martensite phases in 304 stainless steel," *Metall. Trans.*, **1** 1577–1586 (1970).

[25] S. S. Hecker, M. G. Stout, K. P. Staudhammer, and J. L. Smith, "Effects of strain state and strain rate on deformation-induced transformation in 304 stainless steel: Part i. magnetic measurements and mechanical behavior," *Metall. Trans. A*, 620–626 (1982).

[26] F. A. Garner, "Radiation damage in austenitic steels"; pp. 33–95 in *Comprehensive Nuclear Materials*, Elsevier, Amsterdam, 2012.

[27] G. B. Olson and M. Cohen, "General mechanism of martensitic nucleation: part II. FCC->BCC and other martensitic transformations," *Metall. Trans. A*, **7A** 1905–1914 (1976).

[28] A. J. Bogers and W. G. Burgers, "Partial dislocations on the $\{110\}$ planes in the b.c.c. lattice and the transition of the f.c.c. into the b.c.c. lattice," *Acta Metall.*, **12** 255–261 (1964).

[29] M. Bauccio, *ASM Metals Reference Book*, 3rd edition; pp. 379–434, American Society for Metals, Materials Park, Ohio, 1993.

[30] G. L. Hankin, M. B. Toloczko, M. L. Hamilton, F. A. Garner, and R. G. Faulkner, "Shear punch testing of 59Ni isotopically-doped model austenitic alloys after irradiation in FFTF at different He/dpa ratios," *J. Nucl. Mater.*, **258-263** 1657–1663 (1998).